

This is an Open Access document downloaded from ORCA, Cardiff University's institutional repository: <https://orca.cardiff.ac.uk/id/eprint/134325/>

This is the author's version of a work that was submitted to / accepted for publication.

Citation for final published version:

Wu, Haoliang, Jin, Fei , Bo, Yulin, Du, Yanjun and Zheng, Junxing 2018. Leaching and microstructural properties of lead contaminated kaolin stabilized by GGBS-MgO in semi-dynamic leaching tests. *Construction and Building Materials* 172 , pp. 626-634. [10.1016/j.conbuildmat.2018.03.164](https://doi.org/10.1016/j.conbuildmat.2018.03.164)

Publishers page: <https://doi.org/10.1016/j.conbuildmat.2018.03.164>

Please note:

Changes made as a result of publishing processes such as copy-editing, formatting and page numbers may not be reflected in this version. For the definitive version of this publication, please refer to the published source. You are advised to consult the publisher's version if you wish to cite this paper.

This version is being made available in accordance with publisher policies. See <http://orca.cf.ac.uk/policies.html> for usage policies. Copyright and moral rights for publications made available in ORCA are retained by the copyright holders.



Manuscript Number: CONBUILDMAT-D-18-00341R1

Title: Leaching and Microstructural Properties of Lead Contaminated  
Kaolin Stabilized by GGBS-MgO in Semi-Dynamic Leaching Tests

Article Type: Research Paper

Keywords: Slag; reactive MgO; leaching test; contaminated soil;  
solidification/stabilization

Corresponding Author: Professor YanJun Du, PhD

Corresponding Author's Institution: Southeast University

First Author: H.L. Wu

Order of Authors: H.L. Wu; F. Jin; Y.L. Bo; YanJun Du, PhD; J.X. Zheng

Abstract: Ground granulated blast furnace slag (GGBS) is widely used to stabilize soils due to its environmental and economic merits. The strength and durability of reactive MgO activated GGBS (GGBS-MgO) stabilized lead (Pb)-contaminated soils have been explored by previous studies. However, the effects of simulated acid rain (SAR) on the leachability and micro-properties of GGBS-MgO stabilized Pb-contaminated soils are hardly investigated. This research studies the leachability and microstructural properties of GGBS-MgO stabilized Pb-contaminated kaolin clay exposed to SAR with initial pH values of 2.0, 4.0 and 7.0. A series of tests are performed including the semi-dynamic leaching tests using SAR as the extraction liquid, acid neutralization capacity (ANC), mercury intrusion porosimetry (MIP), and X-ray diffraction (XRD) tests. The results demonstrate that as the SAR pH decreases from 7.0 to 4.0, the cumulative fraction leached (CFL) and observed diffusion coefficient (Dobs) of Pb increases significantly. Meanwhile, increasing the GGBS-MgO content from 12% to 18% results in decrease of CFL and Dobs. Further decreasing the SAR pH to 2.0 results in the dissolution-controlled leaching mechanism and more notable increase in CFL regardless of the binder dosage. The differences in the leaching properties under different pH conditions are interpreted based on the cemented soil acid buffering capacity, hydration products and pore size distributions obtained from the ANC, MIP, and XRD tests, respectively.

### Research Highlights:

- Leaching is diffusion-controlled at pH 7 and 4 while dissolution-controlled at pH 2
- Observed diffusion coefficient is affected by the SAR pH and binder dosage
- Pb is primarily precipitated as hydrocerussite ( $\text{Pb}_2(\text{CO}_3)_2(\text{OH})_2$ ) in soil matrix
- ANC and pore structure of the treated soil affect diffusive properties of Pb



31 **Abstract:** Ground granulated blast furnace slag (GGBS) is widely used to stabilize soils due  
32 to its environmental and economic merits. The strength and durability of reactive MgO  
33 activated GGBS (GGBS-MgO) stabilized lead (Pb)-contaminated soils have been explored by  
34 previous studies. However, the effects of simulated acid rain (SAR) on the leachability and  
35 micro-properties of GGBS-MgO stabilized Pb-contaminated soils are hardly investigated.  
36 This research studies the leachability and microstructural properties of GGBS-MgO stabilized  
37 Pb-contaminated kaolin clay exposed to SAR with initial pH values of 2.0, 4.0 and 7.0. A  
38 series of tests were performed including the semi-dynamic leaching tests using SAR as the  
39 extraction liquid, acid neutralization capacity (ANC), mercury intrusion porosimetry (MIP),  
40 and X-ray diffraction (XRD) tests. The results demonstrate that as the SAR pH decreases  
41 from 7.0 to 4.0, the Pb cumulative fraction leached (*CFL*) and observed diffusion coefficient  
42 ( $D^{obs}$ ) increases significantly whereas the leachate pH decreases. Meanwhile, increasing the  
43 GGBS-MgO content from 12% to 18% results in the decrease of *CFL* and  $D^{obs}$ . Further  
44 decreasing the SAR pH to 2.0 results in the dissolution-controlled leaching mechanism  
45 regardless of the binder dosage. The differences in the leaching properties under different pH  
46 conditions are interpreted based on the cemented soil acid buffering capacity, hydration  
47 products and pore size distributions obtained from the ANC, MIP, and XRD tests,  
48 respectively.

49

50 **Keywords:** Slag; reactive MgO; leaching test; contaminated soil; solidification/stabilization

## 51 **1 Introduction**

52 Numerous abandoned industrial sites worldwide have been found to be  
53 contaminated with a wide range of heavy metals [1-7]. These toxic metals such as  
54 lead (Pb), zinc (Zn), copper (Cu), and cadmium (Cd), if treated improperly, can pose  
55 severe threats to the environment and human health. Considering the fast urbanization  
56 and ever-increasing value of the land resources, particularly in the developing  
57 countries such as China and India, it is imperative to develop effective and  
58 economical technologies to remediate these heavy metal contaminated industrial sites.  
59 The ultimate goal is to eliminate their negative environmental impact to the society  
60 and improve the mechanical properties of soils to facilitate post-construction.  
61 Solidification/Stabilization (S/S) has been widely used to immobilize contaminants  
62 and improve the soil properties [2-3, 8]. After S/S, the remediated soils can be reused  
63 in-situ as engineering construction materials, which would help on the fast  
64 redevelopment of the contaminated site [9-10].

65 Portland cement (PC) is the most popular binder used in S/S [11]. However, its  
66 manufacturing process is associated with high power consumption (5000 MJ/t PC),  
67 non-renewable resources usage (1.5 t limestone and clay/t PC) and considerable  
68 emissions of carbon dioxide (CO<sub>2</sub>), dust, and deleterious gases (SO<sub>2</sub>, CO, NO<sub>x</sub>) (0.95  
69 t/t PC) [12-13]. Therefore, full or partial replacement of PC by more sustainable  
70 industrial by-products (e.g. fly ash and slag) as alternative binders in treating  
71 contaminated soil has received ever-increasing popularity. One of the promising  
72 alternative binders is alkali-activated slag (AAS) cement using ground granulated

73 blast furnace slag (GGBS) as the main raw material. However, several drawbacks are  
74 associated with the utilization of AAS in S/S including over-rapid setting, difficulty in  
75 handing/transporting the caustic alkalis and uneconomical efficiency [12]. To address  
76 these issues, reactive magnesia (MgO) has been used as an effective activator for the  
77 GGBS [12, 14-16]. Existing studies on the GGBS-MgO binder mainly focus on the  
78 strength, durability and microstructural properties of the pastes and stabilized soils  
79 [14-16]. The MgO facilitates the breakage of Si-O and Al-O bonds in the GGBS to  
80 promote the formation of the calcium silicate hydrate (C-S-H) and hydrotalcite  
81 ( $\text{Mg}_6\text{Al}_2\text{CO}_3(\text{OH})_{16}$ )-like phase (Ht) as the main hydration products [17-19] while  
82 C-S-H and  $\text{Ca}(\text{OH})_2$  are the main hydration products in PC stabilized soils [2,21]. The  
83 C-S-H and Ht formed would enhance the physical and mechanical properties [14-16,  
84 18] and reduce the leachability of contaminants in heavy metal contaminated soils [16,  
85 20]. Recently, the feasibility of using this binder for stabilizing heavy  
86 metal-contaminated soils has been demonstrated both in the laboratory [20] and a  
87 field trial [8]. However, to date, no systematic studies exist on the diffusive properties  
88 of heavy metals in GGBS-MgO stabilized heavy metal contaminated soils.

89 Sharma and Reddy [6] indicated that the acid rain may vary from a highly acidic  
90 condition (pH = 2.0) to a neutral condition (pH = 7.0). It is reported that the average  
91 pH value of the acid rain in Nanjing City, China is about 5.09 with the lowest pH of  
92 2.89 [21-23]. Du et al. [2] and Yun et al. [24] studied the leaching behavior and  
93 long-term durability of PC solidified/stabilized heavy metal-contaminated soils under  
94 various acid rain conditions. They showed that heavy metals could be released

95 notably from the stabilized soils with increased acidity. It is expected that due to the  
96 different hydration chemistry and reaction products formed in GGBS-MgO and PC  
97 binders, the leaching properties of the treated soils exposed to the acid rain would be  
98 different. Therefore, it is necessary to comprehensively evaluate the leaching behavior  
99 of GGBS-MgO stabilized heavy metal-contaminated soils under different acidic  
100 conditions: strongly acidic condition (pH = 2.0), moderate acidic condition (pH = 4.0)  
101 and neutral condition (pH = 7.0).

102 In this study, a series of semi-dynamic leaching tests are performed on lead  
103 (Pb)-contaminated kaolin clay using simulated acid rain as the extraction leachant  
104 with initial pH values of 2.0, 4.0, and 7.0. The effects of acid rain pH and  
105 GGBS-MgO content on the leachability and microstructural properties of the treated  
106 soils are studied. The semi-dynamic leaching test results are interpreted by acid  
107 neutralization capacity (ANC), mercury intrusion porosimetry (MIP) and X-ray  
108 diffraction (XRD). This study provides useful insights for remediating  
109 Pb-contaminated kaolin using the GGBS-MgO binder.

110

## 111 **2 Materials and Testing Methods**

### 112 **2.1 Materials and sample preparations**

113 Kaolin clay is used as a base soil due to its uniform composition (low organic  
114 content, homogeneity and uniform mineralogy) and low cation exchange capacity  
115 [1-3, 14]. The basic physiochemical properties of the kaolin clay are summarized in



116 **Table 1.** The pH is measured per [ASTM D4972 \[25\]](#) using a pH meter HORIBA D-54.  
117 The specific gravity is measured per [ASTM D5550 \[26\]](#). The Atterberg limits are  
118 measured per [ASTM D4318 \[27\]](#). The kaolin clay is classified as lean clay (CL) based  
119 on the Unified Soil Classification System [\[28\]](#). The moisture content is measured as  
120 per ASTM D2216 [\[29\]](#). The grain size distribution is measured using a laser particle  
121 size analyzer Mastersizer 2000.

122 The physiochemical properties of GGBS and MgO are listed in **Table 2**. The  
123 BET specific surface areas of the GGBS and MgO are measured by nitrogen  
124 adsorption using Physisorption Analyzer ASAP2020. The chemical compositions of  
125 the kaolin clay, GGBS, and MgO are measured using X-ray fluorescence (XRF) as  
126 shown in **Table 3**. The reactivity of the MgO is measured as the time duration  
127 required for the neutralization of an acidic solution (0.25 M acetic acid in this study)  
128 by a certain amount of MgO sample (5.0 g in this study) in which phenolphthalein is  
129 adopted as the pH indicator [\[30\]](#). The mean values of the above tests are presented in  
130 **Tables 1 to 3**.

131 Pb is used in this study because it is a very common toxic heavy metal in  
132 contaminated soils [\[3, 14, 31\]](#). Lead nitrate ( $\text{Pb}(\text{NO}_3)_2$ ) powder (Chemical Analytical  
133 Reagent, Sinopharm Chemical Reagent Co., Ltd.) is dissolved in distilled deionized  
134 water (DDW) as stock solutions with predetermined Pb concentrations. The simulated  
135 acid rain (SAR), used as the extraction liquid (leachant) in the semi-dynamic leaching  
136 test, is prepared by diluting nitric acid ( $\text{HNO}_3$ ) and ammonium sulfate ( $(\text{NH}_4)_2\text{SO}_4$ ) in  
137 the DDW. Prior to adding  $\text{HNO}_3$ , ammonium sulfate ( $(\text{NH}_4)_2\text{SO}_4$ ) solution is added to

138 the DDW until the concentration of the sulfate ion ( $\text{SO}_4^{2-}$ ) reaches 0.001 mol/L [2].  
139 The stock solutions of SAR are adjusted to three pH value of 2.0, 4.0, and 7.0  
140 respectively. SAR with pH of 2.0 represents a strong acid rain in the field [2].

141 Previous studies show that a binder with 9: 1 ratio of GGBS to MgO (dry weight  
142 basis) yields relatively higher strength and lower leachability of stabilized  
143 contaminated soils [14]. Therefore, the binder consisting of 90% GGBS and 10%  
144 MgO (dry weight basis) is prepared. Three binder contents are set as 12%, 15%, and  
145 18% (dry weight soil basis) which are typical contents in engineering projects [2]. The  
146 water content and the Pb concentration are set as 45% and 2% (i.e., 20000 mg/kg)  
147 (dry weight soil basis) to simulate a heavily contaminated site soil [11, 21],  
148 respectively. Six mixtures are investigated in total and denoted as  $\text{GM}_i\text{Pb}_j$ , where  $i =$   
149 content of the GGBS-MgO binder (i.e., 12, 15 or 18), and  $j =$  Pb concentration (% , 0  
150 or 2).

151 The kaolin clay, GGBS and MgO powders are placed in a plastic bottle and are  
152 thoroughly mixed by a bench-top mixer. Then the predetermined volume of  $\text{Pb}(\text{NO}_3)_2$   
153 stock solution is added to the plastic bottle and further mixed for 30 minutes by the  
154 mixer to sufficiently homogenize the mixture. The mixture is filled into a cylindrical  
155 PVC mold ( $\Phi 50 \times H 100$  mm) in five equal height layers. The mold is vibrated  
156 manually after each filling to eliminate air bubbles. After five fillings, the mixture is  
157 cured under the standard condition ( $20 \pm 2^\circ\text{C}$ , relative humidity = 95%) for 28 days.  
158 In addition, the GGBS-MgO cement paste (GGBS : MgO = 9:1, water : cement = 0.6)  
159 is prepared following the same procedure but without adding kaolin clay and

160  $\text{Pb}(\text{NO}_3)_2$  solution. Totally six identical soil samples are prepared with four samples  
161 subjected to the semi-dynamic leaching test, and two samples used for the  
162 measurement of specific gravity, water content and density before and after the  
163 semi-dynamic leaching test. The crushed and sieved sample was also used for ANC  
164 and XRD tests. In addition, one GGBS-MgO paste sample is prepared for XRD test.

165 In the authors' previously studies [2, 14], contaminated soils were prepared by  
166 spiking clean soil with heavy metal solution at controlled water content, and cured  
167 under controlled condition ( $20 \pm 2^\circ\text{C}$ , relative humidity = 95%) until chemical  
168 equilibrium between soil and heavy metal is achieved. The mixture is then thoroughly  
169 mixed with binder with designed dosage, compacted under controlled dry density and  
170 water content, and cured before subjected to various tests. The soil sample preparation  
171 method presented in this study is more time effective but the chemical reaction  
172 between Pb and kaolin may not achieve equilibrium, which may influence the  
173 leaching characteristic and microstructural properties of the stabilized soils. Further  
174 study is warranted to address this aspect.

175

## 176 **2.2 Testing Methods**

177 The semi-dynamic leaching test is conducted as per ASTM C1308-08 [32]. Four  
178 replicate samples are tested with three different extraction leachants with pH = 2.0,  
179 4.0, and 7.0, respectively. The ratio of the liquid volume to the solid superficial area is  
180  $9.5 \text{ (mL/cm}^2\text{)}$ . The leachant is replenished at 2 h, 7 h, 1 d and then daily until 11 d. It  
181 is noted that the semi-dynamic leaching test is not conducted for the untreated soil as

182 a preliminary test shown that the untreated soil specimen disintegrated immediately  
183 after soaking in the leachant with pH of 7.0 (i.e., DDW).

184 The pH value of the leachate before each replenishment is measured using a pH  
185 meter HORIBA D-54. An aliquot of the leachate is filtered through a 0.45  $\mu\text{m}$  filter  
186 and acidified to  $\text{pH} < 2.0$  and the concentration of Pb is measured by inductively  
187 coupled plasma optical emission spectrometry (ICP-OES, PerkinElmer Optima 8000).  
188 Triplicate measurements of pH and Pb concentration are conducted for each sample  
189 and the averaged values are reported. The coefficient of variation (COV) values of the  
190 pH and Pb concentration for the triplicate measurements are  $< 3\%$  indicating the good  
191 repeatability of the results. The dry density of each sample is calculated from the  
192 measured water content and density of two reduplicate stabilized soils before and after  
193 the semi-dynamic leaching test.

194 The cumulative mass of leached Pb is calculated by the following equation:

$$195 \quad A_{i,\text{Pb}} = \sum c_i \times V_i \quad (1)$$

196 where  $A_{i, pb}$  = the cumulative mass of leached Pb after  $i$  th leaching (mg),  $c_i$  = the  
197 concentration of Pb after  $i$  th leaching (mg/L), and  $V_i$  = the volume of the leachate (L),  
198 which is 1.66 L in this test. The cumulative fraction of leached mass at time  $t$  ( $CFL$ ) is  
199 calculated by:

$$200 \quad CFL = \frac{A_{i,\text{Pb}}}{m} \quad (2)$$

201 where  $m$  = the total mass of Pb in the specimen (mg). The observed diffusion  
202 coefficient ( $D^{\text{obs}}$ ) is calculated using the following equation:

203 
$$D^{\text{obs}} = \frac{\pi}{4} \left( \frac{CFL}{\sqrt{t}} \cdot \frac{V}{S} \right)^2 \quad (3)$$

204 where  $V$  = volume of the specimen ( $\text{cm}^3$ ),  $S$  = surface area of specimen ( $\text{cm}^2$ ) and  $t$  =  
 205 leaching time (s). Herein,  $D^{\text{obs}}$  is a retarded observed diffusion coefficient since it  
 206 represents both diffusive and sportive properties of the soils [3, 33].

207 ANC test is performed according to the procedures developed by [Stegemann and](#)  
 208 [Côte \[34\]](#). Approximately 10 g soil is sampled from the hand broken sample cured  
 209 under the standard condition for 28 days, crushed, sieved ( $< 100 \mu\text{m}$ ), and mixed with  
 210 100 mL distilled water. A series of titration tests are conducted on the soil-distilled  
 211 water mixture using 0.1 M nitric acid as the extraction liquid. An automatic titrating  
 212 device (Auto Titrator ZDJ-4A) is used to fill extraction liquid until the leachate pH of  
 213 mixture achieves the target value. Approximately 10 mL leachate after each titration  
 214 test is collected and filtered through a  $0.45 \mu\text{m}$  filter, and then the concentration of Pb  
 215 measured by ICP-OES (PerkinElmer Optima 8000). The COV value of the added acid  
 216 volume less than 6%. This test is performed in duplicate and the average results are  
 217 reported.

218 The slope of the titration curve (i.e., acid added to the soil versus leachate pH is  
 219 expressed as an index of  $\beta$  by [Yong \[35\]](#):

220 
$$\beta = - \frac{dC_A}{dpH} \quad (4)$$

221 where  $dC_A$  (cmol) = the increment of moles of acid added to the soil.

222 After the semi-dynamic leaching test, one specimen is used for MIP test  
 223 conducted as per ASTM D4404 [36]. The MIP test is used to determine the pore size

224 distribution of the soil-binder mixture. Approximate 1 cm<sup>3</sup> soil sample is collected  
225 from the specimen's surface to the same depth by carefully cutting with a stainless  
226 steel knife. Then the collected samples are frozen by the liquid nitrogen (boiling point  
227 is -195°C). The frozen samples are dried in a vacuum chamber under -80°C. The MIP  
228 tests are performed on dried samples using an Auto Proe IV 9510 mercury intrusion  
229 porosimeter. The pore diameter is calculated using the following capillary pressure  
230 equation according to ASTM D4404 [36]:

$$231 \quad d = -\frac{4\tau \cos \alpha}{p} \quad (5)$$

232 where  $d$  ( $\mu\text{m}$ ) = pore diameter;  $\tau$  (N/m) = the surface tension;  $\alpha$  ( $^\circ$ ) = contact angles of  
233 mercury with the solid; and  $p$  (N/m<sup>2</sup>) = applied pressure of mercury intrusion. In this  
234 study, the contact angle is set as 139° and surface tension value is set as 4.84×10<sup>-4</sup>  
235 N/mm.

236 The XRD tests are performed on samples of GGBS-MgO paste and 18%  
237 GGBS-MgO stabilized kaolin spiked with 2% Pb that are cured under the standard  
238 condition for 28 days. Prior to the XRD analysis, 10 g sample is collected, air dried,  
239 ground, and sieved (< 0.075 mm), and frozen using liquid nitrogen (-195°C) to be  
240 dried by sublimation of the frozen water at -80°C. The XRD test is conducted on  
241 gold-coated samples on RigakuD/Max-2500 using a Cu-K $\alpha$  source with a wavelength  
242 of 1.5405 Å. The instrument is operated at 40 kV and 20 mA. A step size of  $2\theta = 0.02^\circ$   
243 and a scanning speed of 5 s/step are used in the step scan mode. Samples are analyzed  
244 over a range of  $2\theta$  from 10° to 50°. The binder content, curing time, Pb concentration  
245 and number of replicate samples for the various tests are summarized in **Table 4**.

246

## 247 **3 Results and Analyses**

### 248 **3.1 Dry Density**

249 **Table 5** shows the properties of the Pb-contaminated kaolin clay treated by different  
250 contents of GGBS-MgO before the semi-dynamic leaching test. The water content  
251 and porosity slightly decrease with increasing content of GGBS-MgO, whereas dry  
252 density values are practically the same regardless of GGBS-MgO content. **Tables 6**  
253 **and 7** present the dry density and normalized dry density after leaching under  
254 different SAR pH conditions. It is shown that the change of both dry density and  
255 normalized dry density are insignificantly with GGBS-MgO content or SAR pH.

256

### 257 **3.2 Cumulative Fraction Leached and Leachate pH**

258 **Fig. 1** shows the evolution of the cumulative Pb fraction (*CFL*) and leachate pH  
259 with time for samples with different GGBS-MgO contents under SAR pH = 2.0, 4.0,  
260 and 7.0 . It can be seen that the *CFL* gradually increase throughout the entire leaching  
261 time. When GGBS-MgO content increases from 12 to 18%, *CFL* decreases regardless  
262 of the SAR pH. The binder content only has a marginal influence on the *CFL* when it  
263 exceeds 15%. At the same binder content and time, the increments of *CFL* are much  
264 more significant when SAR pH decreases from 4.0 to 2.0 than those when SAR pH  
265 decreases from 7.0 to 4.0. The observation is consistent with those reported by [2]  
266 where PC is used as the binder for stabilizing Pb-contaminated kaolin soil. When the

267 SAR pH values are 4.0 or 7.0, the leachate pH curves are close to each other and both  
268 are approximately 10.5. When the SAR pH decreases from 4.0 to 2.0, a remarkable  
269 decrease of the leachate pH to ~2.5 is observed because the amount of the alkaline  
270 hydration products formed in the soil matrix is not sufficient to buffer the acid  
271 solution.

272

### 273 **3.3 Observed diffusion coefficient**

274 The cumulative Pb per cross-section area of the soil is plotted against  $\log(t)$  in  
275 **Fig. 2** for different SAR pH values. The slopes of the regression lines are calculated in  
276 **Table 8**. According to USEPA (Method 1315), if the slope is close to 1 (slope  $> 0.65$ ),  
277 surface dissolution will be the dominant leaching mechanism. If the slope is close to  
278 0.5 ( $0.35 < \text{slope} \leq 0.65$ ), diffusion is the leaching mechanism. If the slope is lower  
279 than 0.35, wash-off occurs (or depletion if it is found in the middle or at the end of the  
280 test). This study shows that for SAR pH = 2.0, the leaching mechanism is dissolution  
281 while it is diffusion for SAR pH = 4.0 and 7.0. The observed diffusion coefficients  
282 ( $D^{\text{obs}}$ ) are in the range of  $10^{-18}$  -  $10^{-12}$  m<sup>2</sup>/s, which agree with the results from previous  
283 studies [37-41]. The comparisons of  $D^{\text{obs}}$  for Pb in GGBS-MgO, fly ash,  
284 quicklime-sulfate and PC stabilized soils [37-42] are shown in **Fig. 3**. Only a few  $D^{\text{obs}}$   
285 values exist at leachant pH 2.0 due to the strong dissolution effect. When SAR pH is  
286 4.0 or 7.0,  $D^{\text{obs}}$  decreases as the GGBS-MgO content increases from 12% to 18%. The  
287 main hydration products in the GGBS-MgO binder are calcium silicate hydrate  
288 (C-S-H), hydrotalcite-like phases (Ht) and brucite (Mg(OH)<sub>2</sub>) if there is excess MgO



289 [20]. The formation of brucite and Ht causes a large solid volume expansion and fill  
290 pores in stabilized soils [20], leading to more compacted soil structure [2] and  
291 therefore lower  $D^{\text{obs}}$  with higher binder dosages. When the SAR pH decreases from  
292 7.0 to 4.0, the more aggressive SAR attack on the hydration products leads to their  
293 gradual dissolution and consequently higher porosity (see “MIP test” section),  
294 resulting in slightly higher  $D^{\text{obs}}$ .

295

### 296 3.4 Acid neutralization capacity

297 **Fig. 4(a)** illustrates the titration curves for Pb-contaminated kaolin clay treated  
298 by GGBS-MgO. Before adding the acid, the soil with 12% GGBS-MgO binder  
299 displays a slightly lower leachate pH than that of the soil with 18% GGBS-MgO  
300 binder (i.e., soil pH = 9.9 versus 10.3). Higher GGBS-MgO binder content increases  
301 the initial soil pH and thereby could increase the resistance against acid attack. **Fig.**  
302 **4(b)** shows the values of  $\beta$  computed by **Eq. (4)**. Values of  $\beta$  gradually decrease with  
303 leachate pH dropping from 10.0 to 5.0. The leachates with pH lower than 5.0 are not  
304 appropriate for evaluating the buffering capacity of the contaminated kaolin in this  
305 study since a certain amount of soil minerals might have dissolved in the ANC test  
306 [35]. **Du et al. [14]** stabilized Zn and Pb contaminated soils with a phosphate-based  
307 binder and observed the turning point of  $\beta$  occurs at the leachate pH of 5.0. In **Fig. 4(b)**  
308 the turning point of  $\beta$  is around 7.0 which is slightly higher than **Du et al. [14]** because  
309 the kaolin clay used in this study has less organic component and therefore less acid  
310 buffer capacity than natural clay used by **Du et al. [14]**. **Fig. 4(c)** shows the variation

311 of the leached Pb concentration ( $\mu\text{g}/\text{kg}$  dry soil) with leachate pH obtained from the  
312 ANC test. When the leachate pH is in the range of 2.0 to 4.0, leached Pb  
313 concentration decreases noticeably with the increasing GGBS-MgO content or pH. In  
314 contrast, leached Pb concentration is lower than  $0.015 \mu\text{g}/\text{kg}$  and the values are  
315 practically the same when the leachate pH ranges from 5.0 to 10.0 regardless of the  
316 GGBS-MgO content or leachate pH.

317

### 318 **3.5 Pore size distribution**

319 **Fig. 5** presents the cumulative pore volumes for the Pb-contaminated kaolin clay  
320 treated by 12% and 18% GGBS-MgO under different pH conditions. Under the same  
321 SAR pH condition, the specimens stabilized with 12% GGBS-MgO have notably  
322 larger cumulative pore volume than the specimens stabilized with 18% GGBS-MgO.  
323 At the same GGBS-MgO content, the cumulative pore volume decreases as the SAR  
324 pH increases, which is more noticeable when SAR pH decreases from 4.0 to 2.0.

325 **Fig. 6** shows the pore volumes for pore diameters in different ranges:  $< 0.01 \mu\text{m}$   
326 (intra-aggregate),  $0.01$  to  $10 \mu\text{m}$  (inter-aggregate) and  $> 10 \mu\text{m}$  (air pores) respectively.  
327 This classification of pore sizes is suggested by [Horpibulsuk et al. \[43\]](#) for the cement  
328 and fly ash-stabilized silty clay. The volume percentages of above classified pores are  
329 shown in **Table 9**. Regardless of the GGBS-MgO content, the proportions of air pores  
330 and intra-aggregate pores increase (more noticeable for air pores), whereas those of  
331 inter-aggregate pores decrease when the SAR pH decreases from 7.0 to 2.0.  
332 Increasing GGBS-MgO content is found to decrease the proportions of air pores while

333 increase those of inter- and intra-aggregate pores.

334

### 335 **3.6 X-ray diffraction analysis**

336 XRD tests are conducted on the GGBS-MgO paste and 18% GGBS-MgO  
337 stabilized kaolin spiked with 2% Pb to investigate the emerging reaction products in  
338 the GGBS-MgO paste and stabilized Pb-contaminated kaolin. The results are  
339 presented in **Fig 7**. For GGBS-MgO paste samples, the characteristic peaks of Ht at  
340  $2\theta \approx 11.5^\circ$  and  $22.9^\circ$  agree well with the findings of other researchers [20, 44]. In  
341 addition, C-S-H has been detected at  $2\theta \approx 29.8^\circ$ ,  $31.6^\circ$ ,  $38.0^\circ$  and  $48.7^\circ$ . The C-S-H has  
342 lower ratio of calcium and silicon, and therefore its peak is close to the calcite ( $\text{CaCO}_3$ )  
343 ( $2\theta = 29.8^\circ$ ) as reported by previous studies [20, 44]. MgO is identified suggesting  
344 that it has not been fully consumed after 28 days of curing. For Pb-contaminated  
345 kaolin treated with 18% GGBS-MgO, the  $2\theta$  values of the C-S-H and Ht are found at  
346  $\sim 31.7^\circ$  and  $11.3^\circ$  respectively. The characteristic peak of quartz ( $\text{SiO}_2$ ) has been  
347 detected at  $2\theta \approx 33.6^\circ$ . The  $2\theta$  of the kaolinite is detected at  $2\theta \approx 12.6^\circ$ ,  $19.8^\circ$  and  $34.8^\circ$ .  
348 Additionally, a trace peak of lead carbonated hydroxide hydrate (hydrocerussite,  
349  $\text{Pb}_2(\text{CO}_3)_2(\text{OH})_2$ ) has been detected at  $2\theta = 34.2^\circ$ , which agrees well with Jin and  
350 Al-Tabbaa (2014a) [20] that the main immobilization mechanism for Pb by  
351 GGBS-MgO binder is the formation of hydrocerussite.

352

## 353 **4 Discussion**

354 This study demonstrates that the SAR pH and GGBS-MgO content affect

355 considerably the leachability and  $D^{obs}$  of Pb and microstructural properties of the  
356 GGBS-MgO stabilized Pb-contaminated kaolin clay. The mechanisms controlling the  
357 variation of these features are summarized as follows:

358 (1) As the SAR pH decreases from 7.0 to 2.0, the hydration products (C-S-H and  
359 Ht) and kaolin might have been gradually dissolved although it is not explored in this  
360 study. The treated Pb-contaminated soils subjected to the acidic conditions (pH 4.0 to  
361 2.0), therefore, possess looser structures as compared to those subjected to the neutral  
362 condition (pH 7.0) (**Fig. 6**). As the GGBS-MgO content increases from 12% to 18%,  
363 higher amounts of hydration products have formed in the soil matrix [15] which in  
364 turn results in lower leached Pb concentration observed in the ANC test (**Fig. 4(c)**)  
365 and reduces the cumulative volume of pores and the proportions of air pores obtained  
366 from the MIP analyses (**Fig. 5**). More compact structure leads to lower  $D^{obs}$  and  $CFL$   
367 values of Pb in the stabilized soils [2].

368 (2) Regarding the relative variations of the pore volumes in different sizes  
369 (**Table 9**), it is proposed that: (a) acid attack results in disintegration of the soil-binder  
370 aggregates because kaolin particles and hydration products filling the intra-aggregate  
371 pores dissolve, and therefore the intra-aggregate pores volume is elevated; (b) the  
372 aggregates themselves, which are formed by kaolin-cement clusters, gradually and  
373 partially dissolve due to the acid attack, resulting in the transformation of  
374 inter-aggregate pores to air pores. Hence, the inter-aggregate pores volume decreases  
375 with decreasing SAR pH, whereas the air pores volume increases with decreasing  
376 SAR pH.

377 (3) Different SAR pH conditions and GGBS-MgO contents affect the soil acid  
378 buffering capacity (**Fig. 4**). The  $\beta$  values decreases with decreasing pH because the  
379 more hydration products are dissolved with more free hydrogen ions ( $H^+$ ) in the  
380 extraction liquid. As the GGBS-MgO content increases from 12% to 18%, a higher  
381 concentration of free hydroxyl ions ( $OH^-$ ) are produced in the soil pores due to cement  
382 hydration, resulting in higher  $\beta$  values.

383 (4) Both soil structure and acid buffering capacity affect  $CFL$  and  $D^{obs}$  of Pb. The  
384 above analyses show that soils exhibit loose structures and low  $\beta$  values when SAR  
385 pH or GGBS-MgO content reduces, which in turn results in elevated  $CFL$  values (**Fig.**  
386 **1**). **Eq. (3)** shows that  $D^{obs}$  obtained from the semi-dynamic test has a square  
387 relationship with  $CFL$ . Consequently,  $D^{obs}$  values increase with the decreasing SAR  
388 pH or GGBS-MgO content (**Table 8**). At a strong acidic condition (pH 2.0), leaching  
389 of Pb is controlled by the mineral dissolution process and therefore  $D^{obs}$  is not  
390 available.

391 It should be noted that the stabilized soils are cured for 28 d in this study, while it  
392 is demonstrated that the mechanical properties/microstructure of GGBS-MgO  
393 improve significantly in the long term (> 90 days) [15, 45]. Therefore longer curing  
394 time is warranted to fairly evaluate the performance of GGBS-MgO stabilized  
395 contaminated soils. Moreover, the tested soil samples are prepared under  
396 well-controlled laboratory conditions, so it is suggested that field contaminated soils  
397 could be adopted in future studies.

398

## 399 **5 Conclusions**

400 This study investigates the effect of acid rain with different pH values on the  
401 leaching properties of GGBS-MgO stabilized Pb-contaminated kaolin clay via a series  
402 of semi-dynamic leaching tests. The effects of the pH of simulated acid rain (SAR)  
403 and GGBS-MgO content on the cumulative fraction leached (CFL), observed  
404 diffusion coefficient of Pb and pore size distribution profiles of the soils are  
405 investigated. Based on the results obtained from this study, the following conclusions  
406 can be drawn:

407 (1) The changes of dry density and normalized dry density of Pb-contaminated  
408 kaolin clay with GGBS-MgO content or acid rain pH are insignificant within the  
409 test conditions in this study.

410 (2) The *CFL* of Pb is notably affected by the simulated acid rain pH and  
411 GGBS-MgO content. *CFL* decreases with increasing GGBS-MgO content while  
412 increases with decreasing pH, and its increment is more notable at pH 2.0. At pH  
413 2.0, mineral dissolution is found to be the dominant process that controls the  
414 leaching of Pb.

415 (3) The dominant leaching mechanism of Pb is diffusion at pH 4.0 and 7.0.  $D^{obs}$   
416 values of Pb decrease with increasing GGBS-MgO content. The results obtained  
417 from this study and those reported in the literature demonstrate that  $D^{obs}$  values  
418 of Pb increases with decreased pH of leachant tested in the leaching tests.

419 (4) The Pb-contaminated soils with higher GGBS-MgO content display flatter acid  
420 neutralization capacity titration curves and higher acid buffer capacity index.

421 When the leachate pH ranges from 2.0 to 4.0, the leached Pb concentration  
422 obtained from the ANC test decreases noticeably with increasing GGBS-MgO  
423 content or leachate pH, while it changes insignificantly regardless of  
424 GGBS-MgO content or leachate pH when pH is in the range of 5.0 to 10.0.

425 (5) MIP results show that the cumulative pore volume decreases as the simulated  
426 acid rain pH or GGBS-MgO content increases. The volume percentages of air  
427 pores and intra-aggregate pores increase while that of inter-aggregate pores  
428 decreases with decreased SAR pH. Increasing GGBS-MgO content decreases the  
429 volume percentages of air pores while increases those of both inter- and  
430 intra-aggregate pores.

431 (6) Lead is primarily precipitated as hydrocerussite ( $\text{Pb}_2(\text{CO}_3)_2(\text{OH})_2$ ) in the soil  
432 matrix after GGBS-MgO treatment. The acid buffer capacity and pore structure  
433 obtained from the ANC test and MIP analyses are essential for interpreting  
434 effects of leachant pH and GGBS-MgO content on the leachability and diffusive  
435 properties of Pb in the soils tested.

436

### 437 **Acknowledgments**

438

439 Financial support for this research is obtained from the Environmental Protection  
440 Scientific Research Project of Jiangsu Province (Grant No. 2016031), National  
441 Natural Science Foundation of China (Grant No. 41472258), Natural Science  
442 Foundation of Jiangsu Province (Grant No. BK2012022), Key Program of Natural

443 Science Foundation of Jiangsu Province (Grant No.BE2017715), Colleges and  
444 Universities in Jiangsu Province Plans to Graduate Research and Innovation  
445 (KYLX16\_0242), and the Scientific Research Foundation of Graduate School of  
446 Southeast University (Grant No. YBJJ1735)..

447

#### 448 **References**

- 449 [1]. Du, Y.J., Jiang, N.J., Liu, S.Y., Jin, F., Singh, D.N., and Puppala AJ, 2014.  
450 Engineering properties and microstructural characteristics of cement-stabilized  
451 zinc-contaminated kaolin. *Canadian Geotechnical Journal*, **51**(3):289–302. doi:  
452 [10.1139/cgj-2013-0177](https://doi.org/10.1139/cgj-2013-0177).
- 453 [2]. Du, Y.J., Wei, M.L., Reddy, K.R., Liu, Z.P. and Jin, F., 2014. Effect of acid rain  
454 pH on leaching behavior of cement stabilized lead-contaminated soil. *Journal of*  
455 *Hazardous Materials*, **271**, 131-140. doi:[10.1016/j.jhazmat.2014.02.002](https://doi.org/10.1016/j.jhazmat.2014.02.002).
- 456 [3]. Du, Y.J., Wei, M.L., Reddy, K.R., Jin, F., Wu, H.L. and Liu, Z.B., 2014. New  
457 phosphate-based binder for stabilization of soils contaminated with heavy metals:  
458 Leaching, strength and microstructure characterization. *Journal of Environmental*  
459 *Management*, **146**, 179-188. doi:[10.1016/j.jenvman.2014.07.035](https://doi.org/10.1016/j.jenvman.2014.07.035).
- 460 [4]. Yang Y.L., Reddy K.R., Du Y.J., Fan RD 2017. Short-term hydraulic  
461 conductivity and consolidation properties of soil-bentonite backfills exposed to  
462 CCR-impacted groundwater. *ASCE Journal of Geotechnical and*  
463 *Geoenvironmental Engineering*. doi: [10.1061/\(ASCE\)GT.1943-5606.0001877](https://doi.org/10.1061/(ASCE)GT.1943-5606.0001877).



- 464 [5]. Hu, L., Meegoda, J.N., Du, J., Gao, S. and Wu, X., 2011. Centrifugal study of  
465 zone of influence during air-sparging. *Journal of Environmental Monitoring*,  
466 **13**(9), 2443-2449. doi: [10.1039/C0EM00594K](https://doi.org/10.1039/C0EM00594K). 111
- 467 [6]. Sharma, H.D. and Reddy, K.R., 2004. *Geoenvironmental engineering: site*  
468 *remediation, waste containment, and emerging waste management technologies.*  
469 John Wiley & Sons, Inc.
- 470 [7]. Yang Y. L., Reddy K.R., Du Y.J., Fan RD., 2017. SHMP amended calcium  
471 bentonite for slurry trench cutoff walls: workability and microstructure  
472 characteristics. *Canadian Geotechnical Journal*.doi: [10.1139/cgj-2017-0291](https://doi.org/10.1139/cgj-2017-0291).
- 473 [8]. Jin, F., Wang, F. and Al-Tabbaa, A., 2016. Three-year performance of in-situ  
474 solidified/stabilised soil using novel MgO-bearing binders. *Chemosphere*, **144**,  
475 681-688. doi: [10.1016/j.chemosphere.2015.09.046](https://doi.org/10.1016/j.chemosphere.2015.09.046).
- 476 [9]. Scanferla, P., Ferrari, G., Pella, R., Ghirardini, A.V., Zanetto, G. and Libralato,  
477 G., 2009. An innovative stabilization/solidification treatment for contaminated  
478 soil remediation: demonstration project results. *Journal of Soils and Sediments*,  
479 **9**(3), 229-236. doi: [10.1007/s11368-009-0067-z](https://doi.org/10.1007/s11368-009-0067-z).
- 480 [10]. Wei, M.L., Du, Y.J., Reddy, K.R. and Wu, H.L., 2015. Effects of freeze-thaw  
481 on characteristics of new KMP binder stabilized Zn-and Pb-contaminated soils.  
482 *Environmental Science and Pollution Research*, 22(24), 19473-19484. doi:  
483 [10.1007/s11356-015-5133-z](https://doi.org/10.1007/s11356-015-5133-z).
- 484 [11]. Chen, L., Du, Y.J., Liu, S.Y. and Jin, F., 2010. Evaluation of cement  
485 hydration properties of cement-stabilized lead-contaminated soils using electrical

- 486 resistivity measurement. *Journal of Hazardous, Toxic, and Radioactive Waste*,  
487 **15**(4), 312-320. doi: [10.1061/\(ASCE\)HZ.1944-8376](https://doi.org/10.1061/(ASCE)HZ.1944-8376).
- 488 [12]. Chen, E. Y., and Li, T. Z., 2011. The ecological environmental effect of high  
489 quality blast furnace slag powder. *China Concrete*, **5**, 24–28.
- 490 [13]. Chen, Q. D., 2001. Use new technology building cement industry of  
491 environmental material type. *Cement Engineering*, **1**, 1–3
- 492 [14]. Du, Y.J., Bo, Y.L., Jin, F. and Liu, C.Y., 2016. Durability of reactive  
493 magnesia-activated slag-stabilized low plasticity clay subjected to drying–wetting  
494 cycle. *European Journal of Environmental and Civil Engineering*, **20**(2), 215-230.  
495 doi:[10.1080/19648189.2015.1030088](https://doi.org/10.1080/19648189.2015.1030088).
- 496 [15]. Jin, F., Gu, K. and Al-Tabbaa, A., 2015. Strength and hydration properties of  
497 reactive MgO-activated ground granulated blastfurnace slag paste. *Cement and  
498 Concrete Composites*, **57**, 8-16. doi:[10.1016/j.cemconcomp.2014.10.007](https://doi.org/10.1016/j.cemconcomp.2014.10.007).
- 499 [16]. Goodarzi, A.R. and Movahedrad, M., 2017. Stabilization/solidification of  
500 zinc-contaminated kaolin clay using ground granulated blast-furnace slag and  
501 different types of activators. *Applied Geochemistry*, **81**, 155-165.  
502 doi:[10.1016/j.apgeochem.2017.04.014](https://doi.org/10.1016/j.apgeochem.2017.04.014).
- 503 [17]. Yi, Y., Liska, M., Al-Tabbaa, A., 2013. Properties of two model soils  
504 stabilized with different blends and contents of GGBS, MgO, lime, and PC.  
505 *Journal of Materials in Civil Engineering*, **26**, 267-274. doi:  
506 [10.1061/\(ASCE\)MT.1943-5533.0000806](https://doi.org/10.1061/(ASCE)MT.1943-5533.0000806).
- 507 [18]. Yi, Y., Liska, M., Al-Tabbaa, A., 2014. Properties and microstructure of

- 508 GGBS-MgO pastes. *Adv. Cem. Res.* 26, 114–122. doi: [10.1680/adcr.13.00005](https://doi.org/10.1680/adcr.13.00005).
- 509 [19]. Wu, X., Jiang, W., Roy, D. M. 1990. Early activation and properties of slag  
510 cement. *Cement and Concrete Research*, 20(6): 961-974.
- 511 [20]. Jin, F. and Al-Tabbaa, A., 2014. Evaluation of novel reactive MgO activated  
512 slag binder for the immobilisation of lead and zinc. *Chemosphere*, **117**, 285-294.  
513 doi: [10.1016/j.chemosphere.2014.07.027](https://doi.org/10.1016/j.chemosphere.2014.07.027).
- 514 [21]. Du, Y.J., Jiang, N.J., Shen, S.L. and Jin, F., 2012. Experimental investigation  
515 of influence of acid rain on leaching and hydraulic characteristics of  
516 cement-based solidified/stabilized lead contaminated clay. *Journal of Hazardous*  
517 *Materials*, **225**, 195-201. doi: [10.1016/j.jhazmat.2012.04.072](https://doi.org/10.1016/j.jhazmat.2012.04.072).
- 518 [22]. Liang, J., 2008. A study on effects of acid rain on soil, yield, and quality on  
519 farming of crops in Nanjing (Doctoral dissertation, PhD Thesis, Nanjing  
520 University of Information Science and Technology).
- 521 [23]. Nanjing Environment Protection Administration (Nanjing EPA). 2012.  
522 Report on the State of Environment in Nanjing, Nanjing Environment Protection  
523 Administration
- 524 [24]. Yun, S.W. and Yu, C., 2015. Immobilization of Cd, Zn, and Pb from soil  
525 treated by limestone with variation of pH using a column test. *Journal of*  
526 *Chemistry*, doi: [10.1155/2015/641415](https://doi.org/10.1155/2015/641415)
- 527 [25]. ASTM. 2001. Standard test method for pH of soils. ASTM standard  
528 D4972-01. American Society for Testing and Materials, West Conshohocken, PA.
- 529 [26]. ASTM. 2014. Standard test method for specific gravity of soil solids by gas

530 pycnometer. ASTM standard D5550-14. American Society for Testing and  
531 Materials, West Conshohocken, PA.

532 [27]. ASTM. 2010. Standard test method for Liquid Limit, Plastic Limit, and  
533 Plasticity Index of Soils. ASTM standard D4318-10. American Society for  
534 Testing and Materials, West Conshohocken, PA.

535 [28]. ASTM. 2011. Standard Practice for Classification of Soils for Engineering  
536 Purposes (Unified Soil Classification System). ASTM standard D2487-11.  
537 American Society for Testing and Materials, West Conshohocken, PA.

538 [29]. ASTM. 2010. Standard Test Methods for Laboratory Determination of Water  
539 (Moisture) Content of Soil and Rock by Mass. ASTM standard D2216-10.  
540 American Society for Testing and Materials, West Conshohocken, PA.

541 [30]. Jin, F. and Al-Tabbaa, A., 2014. Characterisation of different commercial  
542 reactive magnesia. *Advances in Cement Research*, **26**(2), 101-113. doi:  
543 [10.1680/adcr.13.00004](https://doi.org/10.1680/adcr.13.00004).

544 [31]. Xie, J. and Li, F., 2010. Overview of the current situation on brownfield  
545 remediation and redevelopment in China (No. 2933). The World Bank.

546 [32]. ASTM. 2008. Standard Test Method for Accelerated Leach Test for Diffusive  
547 Releases from Solidified Waste and a Computer Program to Model Diffusive,  
548 Fractional Leaching from Cylindrical Waste Forms. ASTM standard C1308-08.  
549 American Society for Testing and Materials, West Conshohocken, PA

550 [33]. Rowe, R.K., Quigley, R.M., Brachman, R.W. and Booker, J.R., 2004. Barrier  
551 systems for waste disposal facilities. Spon Press.

- 552 [34]. Stegemann, J.A. and Cote, P.L., 1991. Investigation of Test Methods for  
553 Solidified Waste Evaluation, Appendix B: Test Methods for Solidified Waste  
554 Evaluation. Environment Canada Manuscript Series, Document T5-15,  
555 Burlington, Ontario, Canada, 49-52.
- 556 [35]. Yong, R.N., 2000. Geoenvironmental Contaminated Soils, Pollutant Fate,  
557 and Mitigation. CRC Press. Taylor & Francis Group.
- 558 [36]. ASTM. 2010. Standard test method for determination of pore volume and  
559 pore volume distribution of soil and rock by mercury intrusion porosimetry,  
560 ASTM Standards D4404-10, 12.01, American Society for Testing and Materials,  
561 West Conshohocken, PA.
- 562 [37]. Liu, Z.P., Du, Y.J., Jiang, N.J., Zhu, J. J., 2013. Leaching properties of  
563 cement-solidified lead-contaminated clay via semi-dynamic leaching tests.  
564 Chinese Journal of Geotechnical Engineering, **35**(12), 2212-2218.
- 565 [38]. Moon, D.H. and Dermatas, D., 2006. An evaluation of lead leachability from  
566 stabilized/solidified soils under modified semi-dynamic leaching conditions.  
567 Engineering Geology, **85**(1), 67-74. doi: [10.1016/j.enggeo.2005.09.028](https://doi.org/10.1016/j.enggeo.2005.09.028).
- 568 [39]. Moon, D.H. and Dermatas, D., 2007. Arsenic and lead release from fly ash  
569 stabilized/solidified soils under modified semi-dynamic leaching conditions.  
570 Journal of Hazardous Materials, **141**(2), 388-394. doi:  
571 [10.1016/j.jhazmat.2006.05.085](https://doi.org/10.1016/j.jhazmat.2006.05.085).
- 572 [40]. Moon, D.H., Dermatas, D. and Grubb, D.G., 2010. Release of arsenic (As)  
573 and lead (Pb) from quicklime-sulfate stabilized/solidified soils under

574 diffusion-controlled conditions. *Environmental Monitoring and Assessment*,  
575 **169**(1), 259-265. doi: [10.1007/s10661-009-1167-3](https://doi.org/10.1007/s10661-009-1167-3).

576 [41]. Song, F., Gu, L., Zhu, N. and Yuan, H., 2013. Leaching behavior of heavy  
577 metals from sewage sludge solidified by cement-based binders. *Chemosphere*,  
578 **92**(4), 344-350. doi: [10.1016/j.chemosphere.2013.01.022](https://doi.org/10.1016/j.chemosphere.2013.01.022).

579 [42]. Alexander, M., Bertron, A. and De Belie, N., 2013. Performance of  
580 cement-based materials in aggressive aqueous environments, RILEM TC  
581 211-PAE. Springer, Berlin.

582 [43]. Horpibulsuk, S., Rachan, R., Chinkulkijniwat, A., Raksachon, Y. and  
583 Suddeepong, A., 2010. Analysis of strength development in cement-stabilized  
584 silty clay from microstructural considerations. *Construction and Building*  
585 *Materials*, **24**(10), 2011-2021. doi: [10.1016/j.conbuildmat.2010.03.011](https://doi.org/10.1016/j.conbuildmat.2010.03.011).

586 [44]. Wang, S.D., and Scrivener, K.L., 1995. Hydration products of alkali  
587 activated slag cement. *Cement and Concrete Research*, **25**(3), 561-571. doi:  
588 [10.1016/0008-8846\(95\)00045-E](https://doi.org/10.1016/0008-8846(95)00045-E).

589 [45]. Gu, K., Jin, F., Al-Tabbaa, A., Shi, B. and Liu, J., 2014. Mechanical and  
590 hydration properties of ground granulated blastfurnace slag pastes activated with  
591 MgO–CaO mixtures. *Construction and Building Materials*, **69**, 101-108. doi:  
592 [10.1016/j.conbuildmat.2014.07.032](https://doi.org/10.1016/j.conbuildmat.2014.07.032).

593

594

## Table Captions

595 **Table 1.** Properties of the kaolin soil used in this study

596 **Table 2.** Main physico-chemical properties of GGBS and MgO

597 **Table 3.** Chemical compositions of the kaolin soil, GGBS and MgO used in this study

598                   measure by XRF

599 **Table 4.** Binder content, curing time, Pb concentration and number of replicated

600                   samples for various tests used in this study

601 **Table 5.** Properties of the stabilized soil before the semi-dynamic leaching tests

602 **Table 6.** Dry density of samples calculated from the measured density and water

603                   content immediately after the semi-dynamic leaching tests

604 **Table 7.** Normalized dry density of samples calculated from the measured density and

605                   water content immediately after the semi-dynamic leaching tests

606 **Table 8.** Calculated  $D^{\text{obs}}$  values and leaching mechanisms of Pb for the soils tested

607                   between 2 h and 11 d

608 **Table 9.** Distribution of the pore volume percentage of the Pb contaminated kaolin

609                   treated by GGBS-MgO after semi-dynamic tests

610

611

612

**Table 1. Properties of the kaolin soil used in this study**

Index	Value
pH	8.77
Specific gravity, $G_s$	2.68
Plastic limit, $w_P$ (%)	14.6
Liquid limit, $w_L$ (%)	29.4
Grain size distribution (%)	
Clay (< 0.002 mm)	21.5
Silt (0.002 to 0.075 mm)	58
Sand (0.075 to 2 mm)	20.5

613



614

**Table 2. Main physico-chemical properties of GGBS and MgO**

Property	Value	
	GGBS	MgO
Alkalinity <sup>a</sup>	1.689	-
Reactivity (s)	-	102
Specific surface area (m <sup>2</sup> /g)	0.2932	28.023
pH (liquid to solid ratio = 1:1)	10.96	10.53

615 <sup>a</sup>The alkalinity of the GGBS is defined as the ratio of contents of CaO, MgO, and  
616 Al<sub>2</sub>O<sub>3</sub> to that of SiO<sub>2</sub>

617

618 **Table 3. Chemical compositions of the kaolin soil, GGBS and MgO used in this**  
 619 **study measure by XRF**

Chemical composition ( <i>wt%</i> )	Kaolin	GGBS	MgO
CaO	0.36	33.08	0.84
Al <sub>2</sub> O <sub>3</sub>	39.3	17.9	0.38
MgO	0.06	6.02	96.5
K <sub>2</sub> O	0.21	0.64	0.01
SiO <sub>2</sub>	52.1	34.3	1.09
Fe <sub>2</sub> O <sub>3</sub>	3.38	1.02	0.19
SO <sub>3</sub>	0.06	1.64	0.26
MnO	0.11	0.28	0.02
TiO <sub>2</sub>	1.12	0.92	0.01
Loss on ignition (at 950°C)	3.3	4.2	0.7

620

621 **Table 4. Binder content, curing times, Pb concentration and number of**  
 622 **replicated samples for various tests used in this study**

Test/ Analysis	Binder content, %	Curing time, days	Pb concentration, %	Number of replicate samples
Dry density	12, 15, 18	28	2	2
Semi-dynamic test	12, 15, 18	28	2	4
ANC <sup>a</sup>	12, 18	28	2	1
MIP <sup>b</sup>	12, 18	28	2	1
XRD <sup>c</sup>	18	28	0, 2	1

623 <sup>a</sup>ANC= Acid neutralization capacity;

624 <sup>b</sup>MIP = Mercury intrusion porosimetry;

625 <sup>c</sup>XRD = X-ray diffraction

626

627

**Table 5. Properties of the stabilized soils before the semi-dynamic leaching tests**

	<sup>a</sup> Specific gravity, $G_s$	<sup>b</sup> Water content, %	Dry density, $\rho_d$ (g/cm <sup>3</sup> )	Porosity, $n$	Saturation degree, $S$
GM12Pb2	2.61	41.0	1.26	0.519	0.992
GM15Pb2	2.59	39.7	1.26	0.514	0.973
GM18Pb2	2.55	38.2	1.28	0.498	0.982

628

<sup>a</sup> ASTM D5550(ASTM 2014)

629

<sup>b</sup> ASTM D2216(ASTM 2010)

630

631 **Table 6. Dry density ( $\text{g}/\text{cm}^3$ ) of samples calculated from the measured density**  
632 **and water content immediately after the semi-dynamic leaching tests**

---

Sample / pH	pH = 2.0	pH = 4.0	pH = 7.0
GM12Pb2	1.20	1.22	1.23
GM15Pb2	1.25	1.25	1.26
GM18Pb2	1.25	1.25	1.26

---

633

634

635 **Table 7. Normalized dry density ( $\text{g/cm}^3$ ) of samples calculated from the measured**  
 636 **density and water content immediately after the semi-dynamic leaching tests**

Sample / pH	pH = 2.0	pH = 4.0	pH = 7.0
GM12Pb2	0.96	0.97	0.98
GM15Pb2	0.99	0.99	1.00
GM18Pb2	0.98	0.98	0.99

637  
 638

639 **Table 8. Calculated  $D^{\text{obs}}$  values and leaching mechanisms of Pb for the soils tested**  
 640 **between 2 h and 11 d**

	pH	Slope	$R^2$	Mechanism	$D^{\text{obs}}$ (m <sup>2</sup> /s)
GM12Pb2	2.0	0.71	0.992	dissolution	-
	4.0	0.51	0.96	diffusion	$1.69 \times 10^{-16}$
	7.0	0.44	0.997	diffusion	$7.67 \times 10^{-18}$
GM15Pb2	2.0	0.8	0.989	dissolution	-
	4.0	0.52	0.972	diffusion	$4.90 \times 10^{-17}$
	7.0	0.58	0.962	diffusion	$5.00 \times 10^{-18}$
GM18Pb2	2.0	0.98	0.982	dissolution	-
	4.0	0.6	0.98	diffusion	$5.07 \times 10^{-17}$
	7.0	0.6	0.948	diffusion	$3.77 \times 10^{-18}$

641

642

643 **Table 9. Distribution of the pore volume percentage of the Pb contaminated**

644 **kaolin treated by GGBS-MgO after semi-dynamic test**

SAR pH	GM12Pb2			GM18Pb2		
	pH = 2.0	pH = 4.0	pH = 7.0	pH = 2.0	pH = 4.0	pH = 7.0
intra-aggregate pores (%)	1.86	1.80	1.77	2.74	2.00	1.76
inter-aggregate pores (%)	90.76	91.18	91.70	91.00	92.15	93.86
air pores (%)	7.38	7.00	6.53	6.26	5.85	4.38

645



## Figure Captions

646

647 **Figure. 1.** CFL for Pb and leachate pH for soils with GGBS-MgO contents of (a) 12%;  
648 (b) 15%; and (c) 18%

649 **Figure. 2.** The plots of cumulative Pb against  $\log(t)$  from the semi-dynamic tests for  
650 specimens with GGBS-MgO content of (a) 12%; (b) 15%; and (c) 18%

651 **Figure. 3.** Variation of  $D^{obs}$  for lead with leachant pH obtained from this study and  
652 previously published studies

653 **Figure. 4.** (a) Acid titration curves; (b) buffer capacity; and (c) leached Pb  
654 concentration of the lead contaminated kaolin clay treated by GGBS-MgO

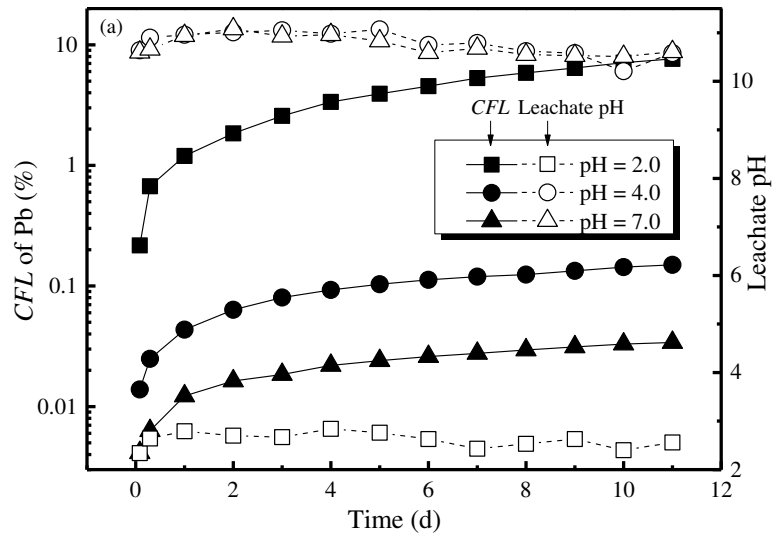
655 **Figure. 5.** Cumulative pore volume of the Pb contaminated kaolin treated by  
656 GGBS-MgO after semi-dynamic leaching test

657 **Figure. 6.** Pore volume percentage of the Pb contaminated kaolin treated by  
658 GGBS-MgO after semi-dynamic test

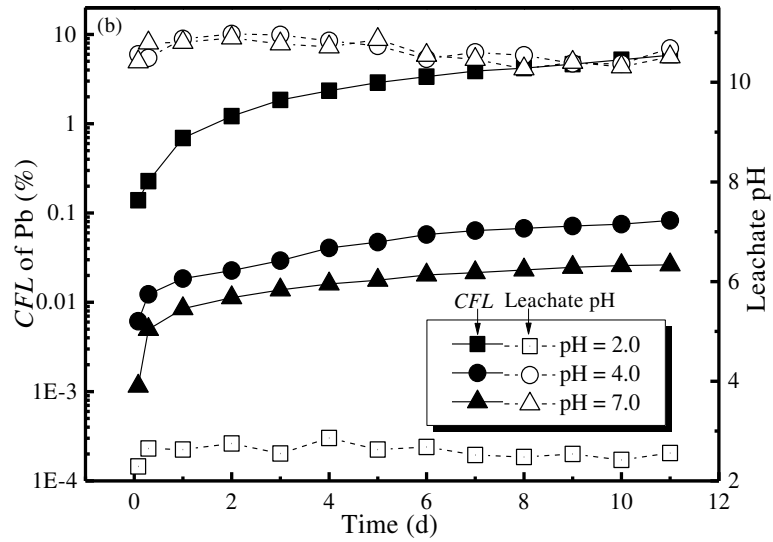
659 **Figure. 7.** X-ray diffractograms of the GGBS-MgO paste and GGBS-MgO treated  
660 Pb-contaminated kaolin cured at the normal condition for 28 days

661

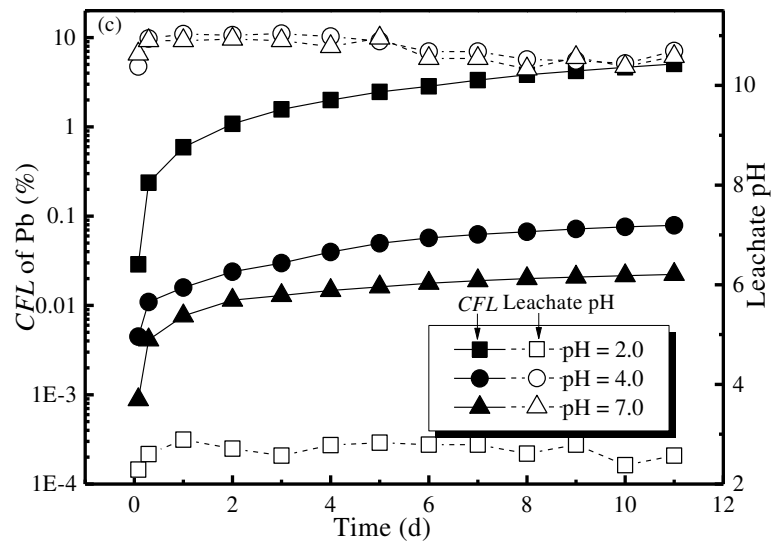
662



663



664



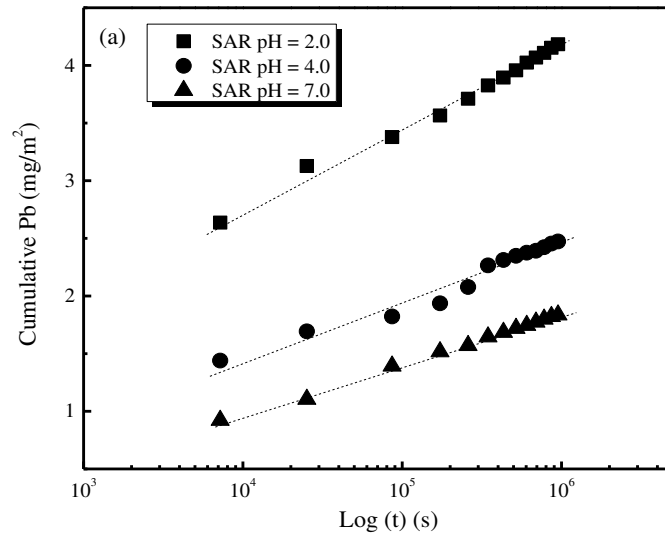
665

666

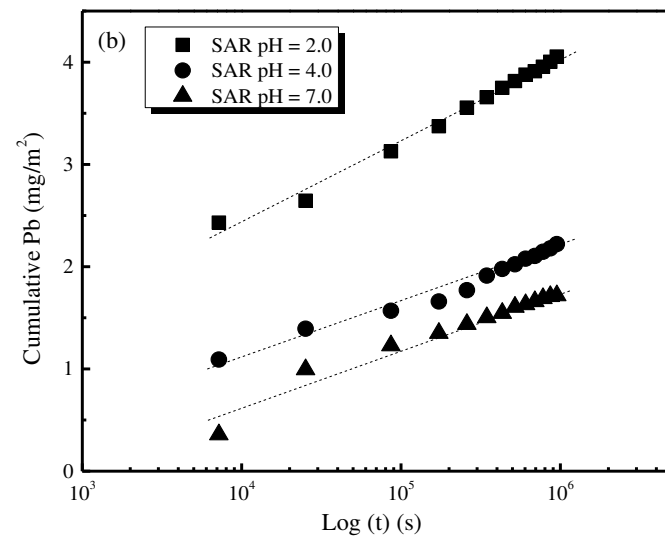
**Fig. 1 CFL for Pb and leachate pH for soils with GGBS-MgO contents of (a)**

667

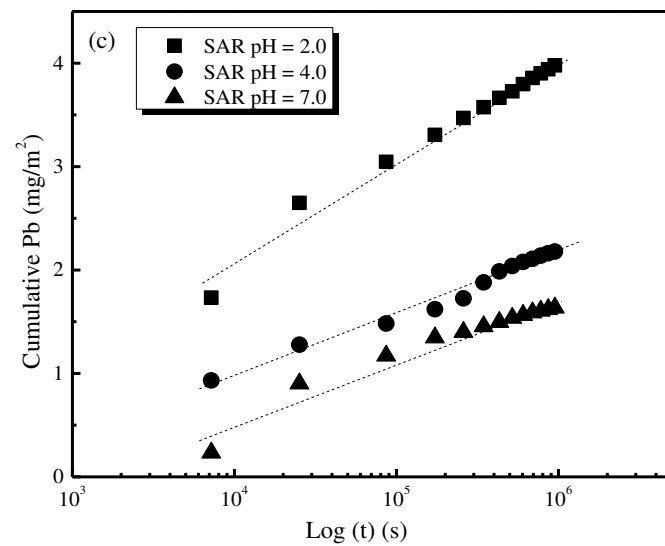
**12%; (b) 15%; and (c) 18%.**



668



669

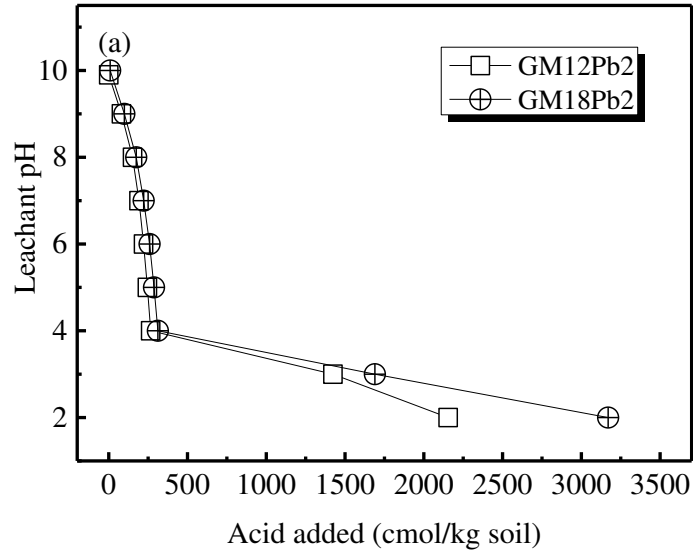


670

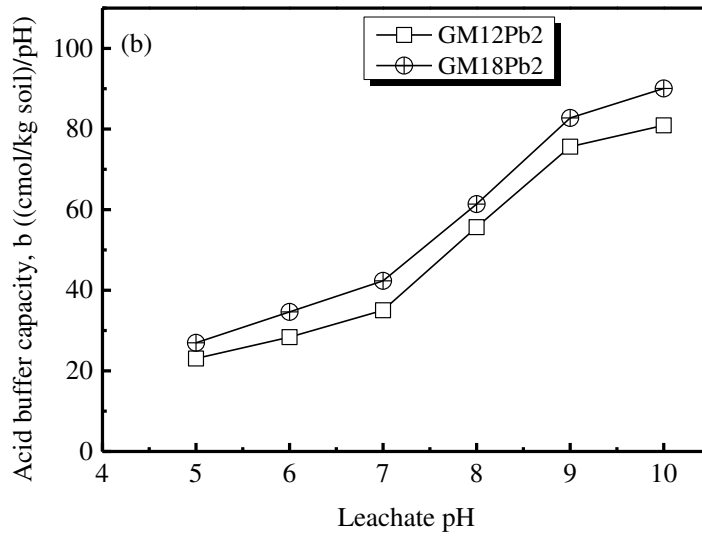
671 **Fig. 2** The plots of cumulative Pb against log (*t*) from the semi-dynamic tests for

672 specimens with GGBS-MgO content of (a) 12%; (b) 15%; and (c) 18%.

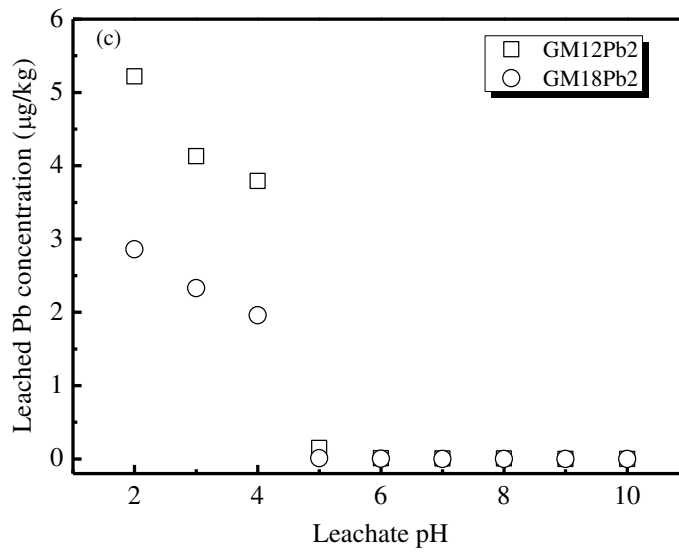




677



678

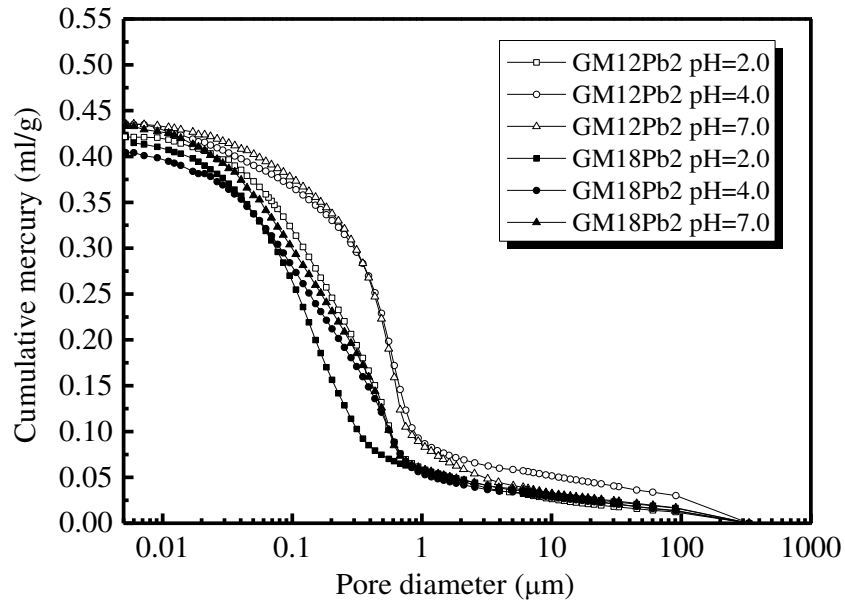


679

680

681

**Fig. 4 (a) Acid titration curves; (b) buffer capacity; and (c) leached Pb concentration of the lead contaminated kaolin clay treated by GGBS-MgO**



682

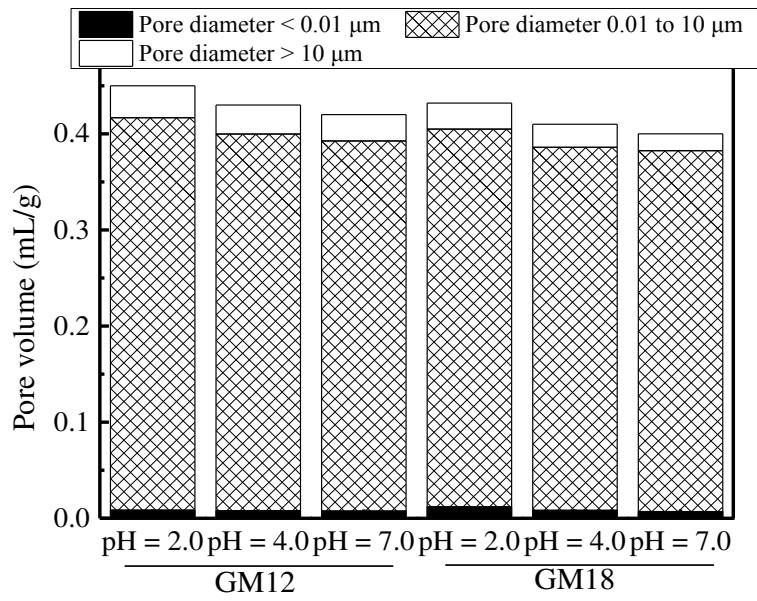
683

**Fig. 5 Cumulative pore volume of the Pb contaminated kaolin treated by**

684

**GGBS-MgO after semi-dynamic leaching test**

685



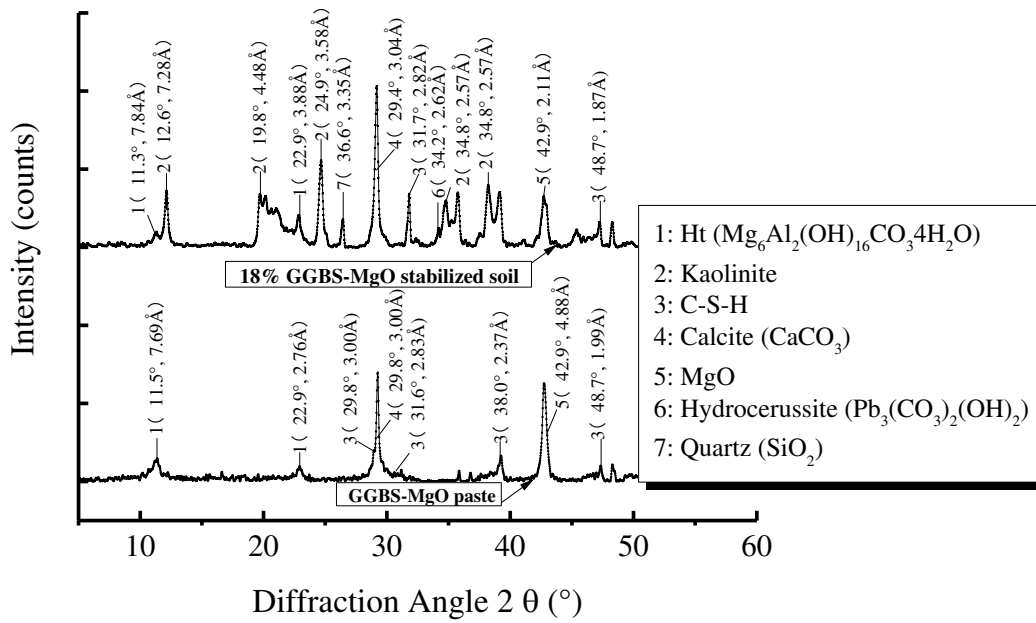
686

687 **Fig. 6 Pore volume percentage of the Pb contaminated kaolin treated by**

688

**GGBS-MgO after semi-dynamic test**

689



690

691 **Fig. 7 X-ray diffractograms of the GGBS-MgO paste and GGBS-MgO treated**

692

**Pb-contaminated kaolin cured under standard condition for 28 days**

693